

## Index

<i>Item</i>	<i>Description</i>	<i>Page</i>
<b>SI Materials and Methods</b>	Protein expression, purification and labeling; details of the ensemble and single-molecule experiments, and data analysis	1
<b>Figure S1</b>	Characterization of phospholipid SUVs	7
<b>Figure S2</b>	Single-molecule characterization of the effect of Hsp27 on SUV binding-coupled-folding of $\alpha$ S.	8
<b>Figure S3</b>	Hsp27 inhibits the interaction of $\alpha$ S with physiologically relevant phospholipid vesicles	9
<b>Note S1</b>	Estimation of concentrations of $\alpha$ S and Hsp27 on the SUV surface	10
<b>Note S2</b>	Characterization of Hsp27-SUV interaction using single-molecule and ensemble fluorescence	11
<b>Figure S4</b>	Characterization of Hsp27-phospholipid vesicle interaction by single-molecule and ensemble fluorescence	12
<b>Note S3</b>	Hsp27 does not interact with the disordered conformation of $\alpha$ S	13
<b>Figure S5</b>	Hsp27 does not interact with the disordered conformation of $\alpha$ S	14
<b>Note S4</b>	Competitive inhibition model for the inhibitory action of Hsp27	15
<b>Figure S6</b>	Comparison of the Hsp27 induced inhibition of $\alpha$ S-SUV interaction with a competitive inhibition model	17
<b>Figure S7</b>	Numerical simulation of the bimodal membrane binding of $\alpha$ S	18
<b>Figure S8</b>	Hsp27 differentially modulates the membrane interaction of the $\alpha$ S <sup>N-ter</sup> and $\alpha$ S <sup>NAC</sup> in the full-length protein	19
<b>Figure S9</b>	A hidden conformation of $\alpha$ S on the lipid bilayer	20
<b>Table S1</b>	Estimated dissociation constants of $\alpha$ S-SUV interactions	21
<b>Supplementary References</b>	References	22

## SI Materials and Methods

Protein expression and purification: *E. Coli* cells (BL21(DE3)) cells were transformed with pET41a plasmid containing human  $\alpha$ -synuclein ( $\alpha$ S) (kindly provided by R. L. Nussbaum (National Institutes of Health, Bethesda, MD)). Transformed cells were induced with IPTG (1 mM final concentration) at OD = 0.6 - 0.8 and further grown for an additional 4 - 6 hrs at 37 °C. Protein extraction was performed using a microfluidizer in lysis buffer (50 mM Tris, 25 mM NaCl, 2 mM EDTA, pH 8.0) containing protease inhibitor cocktail (Roche). Cell debris were removed by centrifugation, followed by nucleic acid precipitation with streptomycin sulfate (Sigma; 1% w/v final concentration; 4 °C, stirring for an hour). The supernatant was further enriched in  $\alpha$ -synuclein using ammonium sulphate (16.6% w/v, 4 °C, stirring for an hour) induced precipitation of bacterial protein impurities, followed by precipitation of  $\alpha$ -synuclein with further addition of ammonium sulphate (additional 12.9 % w/v, 4 °C, stirring for an hour). The pellet was collected by centrifugation (15,000 x g) and dissolved in 10 mM Tris.HCl buffer, pH 7.5. The pH of solution was briefly lowered to 4.5 to induce further precipitation of bacterial proteins<sup>[1]</sup>. The precipitated proteins were removed by centrifugation (15,000 x g), and the pH of the supernatant was changed back to 7.5, followed by buffer exchange to 10 mM Tris, pH 7.5 (to remove any extra salt) using a 3K MWCO centrifugal filter device (Millipore). This solution then was directly loaded onto an anion exchange column (Hitrap Q-HP, GE Healthcare), and the desired protein eluted with a NaCl gradient (0.0-0.5 M). The purity of the sample was checked using SDS-PAGE and ESI-mass spectrometry (Scripps Center for Mass Spectrometry). Protein concentration was determined using an extinction coefficient<sup>[2]</sup> of 5,120 M<sup>-1</sup>. cm<sup>-1</sup>.

The G7C mutant<sup>[3]</sup> of  $\alpha$ S was used for ensemble fluorescence measurements. For initial smFRET experiments, a dual Cys variant, S9C/A85C, was used. plasmid (pET-3a) containing this dual Cys mutant of  $\alpha$ S was kindly provided by S. Lindquist and J. Valastyan (Whitehead Institute, Cambridge, MA). The  $\alpha$ S<sup>N-ter</sup> peptide (with G7C mutation) was purchased from GenScript USA Inc. (NJ, USA). The plasmids (pET-16b) for  $\alpha$ S<sup>NAC</sup> (G84C) and  $\alpha$ S<sup>V3C/G51C</sup> were gene synthesized by GenScript with an N-terminal His<sub>6</sub> tag, followed by a thrombin cleavage site. These proteins were purified as described before<sup>[4]</sup>. Purified proteins contained two exogenous amino acids (GS) from the thrombin recognition sequence at their N-termini. All other mutant proteins were expressed and purified in the same way as the WT protein described above.

Plasmid (pET-20b(+)) containing human Hsp27 (C137A variant) was a kind gift from Hassane S. McHaourab (Vanderbilt University Medical Center, Nashville, TN). The mutation was reversed by site

directed mutagenesis and the resulting construct for the WT Hsp27 was verified for the correct sequence (Eton Bioscience Inc, San Diego, CA), inserted and overexpressed in *E. Coli* cells (BL21(DE3)). Transformed cells were induced with IPTG (1 mM final concentration) at OD = 0.6–0.8 and further grown for an additional 4 - 6 hrs at 37 °C. Protein extraction was performed using a microfluidizer in lysis buffer (50 mM Tris, 25 mM NaCl, 2 mM EDTA, pH 8.0) containing protease inhibitor cocktail (Roche). Cell debris were removed by centrifugation, followed by nucleic acid precipitation by slow addition of 0.05 % PEI (w/v) at 4 °C with constant stirring for an hour. The supernatant was separated from pellet by centrifugation, collected and directly loaded onto an anion exchange column (Hitrap Q-HP, GE Healthcare, and protein was eluted with a NaCl gradient (0.1 - 0.6 M) in 20 mM Tris, pH 8.5. The fractions containing Hsp27 were pooled together, concentrated using a 30K MWCO centrifugal filter device (Millipore), and loaded onto a gel filtration column (Sephacryl S-200 HR, GE Healthcare). The protein was eluted isocratically with 100 mM sodium phosphate buffer, pH 7.5. The fractions containing Hsp27 were further purified by anion exchange chromatography (Hitrap Q-HP, GE Healthcare, Pittsburgh, PA), using a slower NaCl gradient (0.15 - 0.35 M) in 20 mM Tris, pH 8.5. The purity of the sample was checked using SDS-PAGE and ESI-mass spectrometry (Scripps Center for Mass Spectrometry). Protein concentration was determined using an extinction coefficient of 40,450 M<sup>-1</sup>. cm<sup>-1</sup> (protparam: [www.expasy.org](http://www.expasy.org)). For smFRET experiments, G84C/A173C mutant of Hsp27 was produced from the C137A variant by site-directed mutagenesis. The mutant protein was expressed and purified in the same way as the WT protein described above.

Protein labeling: The labeling of  $\alpha$ S mutants for ensemble (mono labeling with G7C and G84C, respectively) and smFRET (dual labeling with 9/85C and 3/51C, respectively) using Cys-maleimide chemistry were carried out as described previously<sup>[4]</sup>. Dual labeling was achieved with a 2-fold molar excess of donor dye (Alexa488 C5-maleimide derivative, Molecular Probes), and 8-fold molar excess of the acceptor dye (Alexa594 C5-maleimide derivative, Molecular Probes) in one pot. For ensemble experiments, either Alexa594 or Alexa488 fluorophore was used to mono-label the  $\alpha$ S variants. For mono-labeling of WT Hsp27 with Alexa594 (C5-maleimide derivative, Molecular Probes) at C137<sup>[5]</sup>, the reaction was carried out in 20 mM Tris, 100 mM NaCl, pH 7.5 at 37 °C for 16 hrs at dark. For mono-labeled samples, the labeling efficiency for all the samples were observed to be  $\geq 90\%$  (UV-Vis absorption measurements), and no additional attempt was made to purify them further, given that only labeled protein is observed in the experiments. Dual labeling of Hsp27 was achieved with a 2-fold molar excess of donor dye (Alexa488 C5-maleimide derivative, Molecular Probes), and 8-fold molar excess of

the acceptor dye (Alexa594 C5-maleimide derivative, Molecular Probes) in one pot in 20 mM Tris, 100 mM NaCl, 4 M Gdn.HCl, pH 7.5 at 4 °C for overnight at dark. The excess dye in all labeling reactions were removed by multiple rounds of washing with the labeling buffers using a 3K MWCO centrifugal filter device (Millipore). The dual-labeled samples were further purified by HPLC with a C4 column. The purity of all the samples (including non-specific dye-binding) were checked by SDS-PAGE and LC-MS (Scripps Center for Mass Spectrometry).

Phospholipid vesicle preparation: The following lipids were used for preparing small unilamellar vesicles (SUVs) used in this study: 1-palmitoyl-2-oleoyl-*sn*-glycero-3-phospho-(1'-*rac*-glycerol) (sodium salt; POPG), 1-palmitoyl-2-oleoyl-*sn*-glycero-3-phosphate (sodium salt; POPA), 1-palmitoyl-2-oleoyl-*sn*-glycero-3-phospho-L-serine (sodium salt; POPS) and 1-palmitoyl-2-oleoyl-*sn*-glycero-3-phosphocholine (POPC). All the lipids were purchased as dissolved in chloroform from Avanti Polar Lipids, Inc (Alabaster, AL). The desired amount of lipids from the stock solutions were taken in a round bottom flask, dried under a gentle stream of nitrogen flow, followed by drying under vacuum for an additional 60 minutes to remove any residual chloroform. The dried lipids were hydrated with 0.2 M NaCl, 10 mM sodium acetate, 10 mM NaH<sub>2</sub>PO<sub>4</sub>, and 10 mM glycine, pH 7.5 (for experiments with  $\alpha$ S) to achieve a final concentration of 2.7 mM. The solution was allowed to sit at room temperature for an hour, followed by vigorous agitation to completely rehydrate the lipids in forming large, multilamellar vesicles with a milky appearance. SUVs were made from this solution by sonication. The appearance of the final solution was almost clear. SUVs were characterized using TEM, which reproducibly showed sizes between 30-70 nm for three independent preparations (Fig. S1).

For the preparation of dye-labeled SUVs for the ensemble vesicle-to-protein FRET assay, Vybrant DiO (3,3'-dioctadecyloxycarbocyanine perchlorate, Molecular Probes) was used. 1 mole % of DiO (1 mM stock solution) was added to the initial solution of lipids in the round bottom flask. The rest of the protocol was the same as described above, except that all the steps were carried out with minimal exposure of light.

Vesicle-binding assay and ensemble fluorescence spectroscopy: To characterize the vesicle binding of proteoms, an ensemble vesicle-to-protein FRET assay was developed. In this assay, phospholipid vesicles were labeled with DiO as donor, and protein samples were labeled with Alexa594 as acceptor. Fluorescence measurements were carried out using an automated temperature controlled PC1 spectrofluorometer (ISS, Champaign, IL) with  $\lambda_{\text{ex}} = 450$  nm in buffer A (0.2 M NaCl, 10 mM sodium

acetate, 10 mM NaH<sub>2</sub>PO<sub>4</sub>, and 10 mM glycine, pH 7.5). To determine the binding curves, a fixed amount of acceptor-labeled protein (250 nM Hsp27) was titrated against variable concentrations of donor-labeled vesicles. Each spectrum was corrected with respect to the same amount of DiO-labeled SUVs in buffer without protein samples.

Steady-state fluorescence anisotropy measurements were performed using the same spectrofluorometer<sup>[6]</sup>. Alexa594-labeled  $\alpha$ S (1  $\mu$ M) was subjected to anisotropy measurements ( $\lambda_{\text{ex}} = 580$  nm, and  $\lambda_{\text{em}} = 618$  nm) in presence of either 0 or 20  $\mu$ M unlabeled Hsp27 in buffer A (0.2 M NaCl, 10 mM sodium acetate, 10 mM NaH<sub>2</sub>PO<sub>4</sub>, and 10 mM glycine, pH 7.5). To determine the binding isotherms of  $\alpha$ S-lipid interaction using anisotropy measurements, dye-labeled  $\alpha$ S (250 nM) was titrated against increasing concentration of POPG SUVs, in presence of fixed amounts of variable concentrations of Hsp27 (see Fig. 1B; Table S1). For Trp fluorescence anisotropy measurements of Hsp27 at increasing concentration of POPG lipids,  $\lambda_{\text{ex}} = 280$  nm, and  $\lambda_{\text{em}} = 350$  nm was used. The protein concentration was 1  $\mu$ M in buffer A in these measurements.

We also evaluated if fluorophores used in this study can non-specifically interact with PG SUVs using fluorescence anisotropy. The anisotropy values of the Alexa dyes in presence of 1000  $\mu$ M POPG remained unchanged (within the measurement error) compared to the values obtained at 0  $\mu$ M POPG. Therefore, we conclude that the anisotropy changes in our anisotropy assay corresponds directly to the protein binding to SUVs, without any significant contribution of the non-specific binding of the fluorescence dyes to the lipid bilayer.

Single-molecule fluorescence spectroscopy: Data collection was done using a home-built confocal microscopy setup as described before<sup>[3, 6]</sup>. Briefly, an Axiovert 2000 microscope (Zeiss, Thornwood, NY) was employed where the sample was excited by focusing the 488-nm line of a 543-AP-A01 tunable argon-ion laser (Melles Griot, Carlsbad, CA) into the sample solution in a Lab-Tek Borosilicate Chambered Coverglass (Nunc, Rochester, NY) using a 1.2 N.A. water immersion objective. The fluorescence emission was detected using SPCM-AQR-14 avalanche photodiode photon counting modules (Perkin-Elmer Optoelectronics, Fremont, CA) after being split into donor and acceptor signals using appropriate dichroic mirrors and filters. Data from the two channels were collected and analyzed to generate FRET efficiency histograms using previously described methods<sup>[3, 6]</sup>. In addition to  $E_{\text{FRET}}$  peaks due to donor to acceptor Förster resonance energy transfer, each histogram contained an additional peak at zero  $E_{\text{FRET}}$  values. This peak can also arise due to the donor-only signals from either dual-donor labelled proteins or proteins with photo-bleached acceptors. All the experiments were

performed at room temperature in buffer A (0.2 M NaCl, 10 mM sodium acetate, 10 mM NaH<sub>2</sub>PO<sub>4</sub>, and 10 mM glycine, pH 7.5) using dual-labeled (either with  $\alpha S^{9/85}$  or  $\alpha S^{3/51}$  construct)  $\alpha S$  at a concentration of  $\sim 100$  pM in the absence or presence of variable amounts of Hsp27, vesicles and SDS, as indicated in the text. For smFRET experiments with Hsp27 (dual labeled at 84/173),  $\sim 100$  pM dual-labeled protein is mixed with an excess (850 nM) of the unlabeled WT protein in the same buffer.

Fluorescence Correlation Spectroscopy (FCS): The confocal smFRET instrumental set-up was used to collect FCS data with Alexa488 labeled  $\alpha S^{G7C}$  with minor modifications to the protocol described previously<sup>[7]</sup>. The protein concentration was 25 nM. The confocal volume was calibrated using the known diffusion coefficient of free Alexa488 fluorophore<sup>[8]</sup>, which yielded the axial and radial dimensions ( $\omega_z$  and  $\omega_{xy}$ ) of our excitation volume as 0.266 and 2.0  $\mu m$ , respectively. The autocorrelation curves were fitted with the following standard equation, with  $i=1$ :

$$G(\tau) = \sum_i \frac{1}{N_i} \left[ \frac{1}{\tau + \tau_D^i} \right] \left[ \frac{1}{\tau + \omega^2 \cdot \tau_D^i} \right]^{0.5} \quad ; \quad \omega = \frac{\omega_z}{\omega_{xy}} \quad (1)$$

Analysis of binding curves and  $K_D$  estimation:  $\alpha S$ -SUV interactions were quantified using smFRET, ensemble steady-state anisotropy and vesicle-to-protein FRET, Hsp27 binding to SUVs were analyzed using ensemble vesicle-to-protein FRET assay, smFRET and Trp fluorescence anisotropy. Determination of binding events using smFRET was done as described in detail in a previous report by Ferreon et al<sup>[6]</sup>. Briefly, population distributions of vesicle bound and unbound  $\alpha S$ /Hsp27 as a function of lipid concentration were directly determined from smFRET histograms (total number of events  $> 300,000$  in individual cases) after they were fitted with Gaussian functions using OriginPro 8.6. The binding isotherms were analyzed and  $K_D$  (defined as [SUV] or [lipid] required for 50% binding) values were estimated with the following equation using OriginPro 8.6:

$$f_b = \frac{[L]}{K_D + [L]} \quad ; \quad f_b = \text{Fraction of protein bound; } L = \text{Lipid} \quad (2)$$

To fit the ensemble anisotropy data, the following equation was used:

$$Y = Y_0 + \frac{(Y_{max} - Y_0) \cdot [L]}{K_D + [L]} \quad ; \quad L = \text{Lipid} \quad (3)$$

For Hsp27, all the binding isotherms were analyzed by non-linear least squares fit of the data to the following logistic Hill equation accounting for sloping baseline in OriginPro 8.6:

$$F_A = y_0 + \frac{(y_{max}-y_0)}{1+10^{\log(n) \cdot (K_D-[L])}}; \quad F_A = \text{Acceptor fluorescence}; L = \text{lipid} \quad (4)$$

We note that modeling the binding curves using Hill and/or transformed-Hill equations for Hsp27 and vesicle interaction may not be straightforward<sup>[9]</sup>. Hsp27 is a oligomeric, highly dynamic and polydispersed protein<sup>[10]</sup>. Moreover, the size of the oligomers of Hsp27 is dependent on the protein concentration and buffer conditions<sup>[11]</sup>, which may also change during ligand interaction. Therefore, we preferred to describe the estimated dissociation constant (defined as [SUV] or [lipid] required for 50% binding) as an apparent dissociation constant ( $K_D^{\text{app}}$ ) for Hsp27-SUV interaction.

## SI Figures

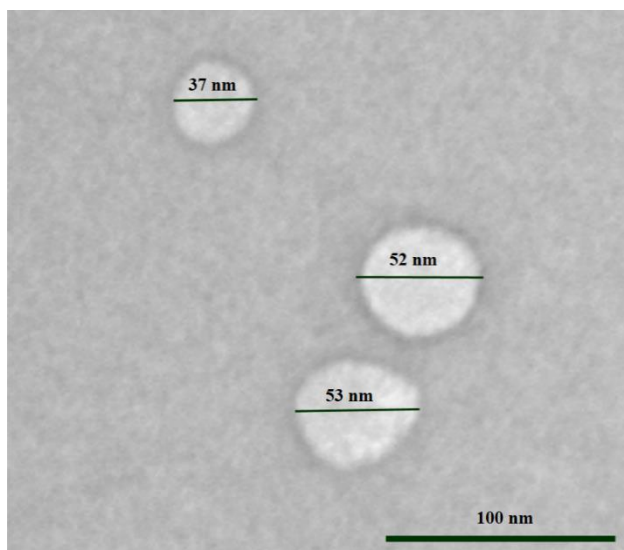


**Figure S1: Characterization of phospholipid SUVs.** Representative electron micrograph of SUVs showing a distribution of different sized vesicles using negative staining TEM. Measurements on three independent SUV preparations yielded an average size of  $49 \pm 18$  nm ( $n = 42$ ).



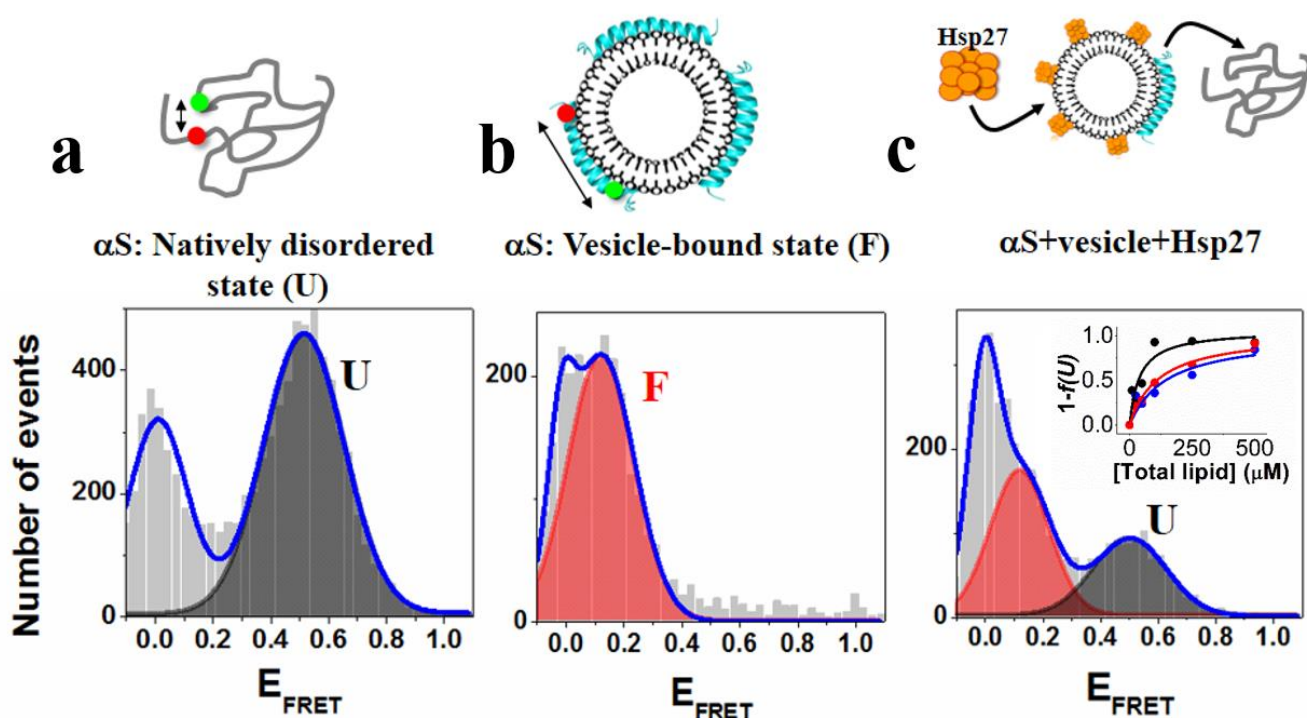


**Figure S2: Single-molecule characterization of the effect of Hsp27 on SUV binding-coupled-folding of  $\alpha$ S.** smFRET histograms of  $\alpha$ S dual-labeled with the Alexa488/Alexa594 FRET dye pair at residues 9 and 85 ( $\alpha$ S<sup>9/85</sup>) showing the (a) disordered U, and (b) extended helical F state of  $\alpha$ S in the absence and presence of 250  $\mu\text{M}$  PG SUV, respectively. (c) Hsp27 (5  $\mu\text{M}$ ) increases the relative population of the U state. Solid lines are Gaussian fits of the data. The *inset* in (c) shows single-molecule binding isotherms ( $f(U)$  = fraction of U state population) for  $\alpha$ S-membrane interaction measured with 0 (black), 1 (red), and 5 (blue)  $\mu\text{M}$  Hsp27. The *arrow* denotes the shift of isotherms as a function of increasing [Hsp27]. The smFRET histograms are compiled using triplicate data sets. A scheme of binding-induced folding of  $\alpha$ S and its inhibition by Hsp27 is shown in the respective top panel. Details on data analysis are described in *SI Methods*.

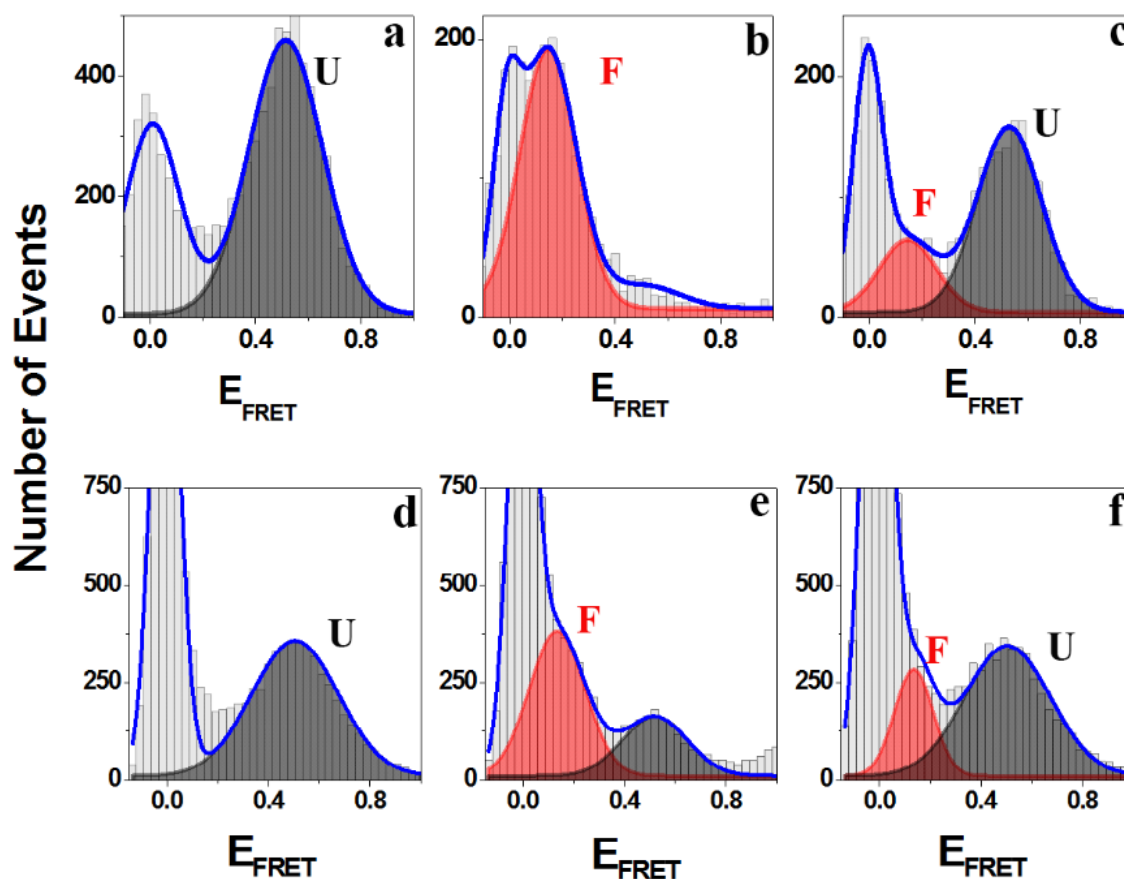


**Figure S3: Hsp27 inhibits the interaction of  $\alpha$ S with physiologically relevant phospholipid vesicles: (a-c) POPA/POPC (50:50) SUVs and (d-f) POPS:POPC (15:85) SUVs.** smFRET histograms showing (a) the disordered U state ( $E_{\text{FRET}} \sim 0.52$ ), and (b) extended helical F state ( $E_{\text{FRET}} \sim 0.15$ ) as predominant conformations of  $\alpha$ S in absence and presence of 250  $\mu\text{M}$  POPA/POPC SUVs, respectively. (c) Shows substantially reduced relative population of the F state of  $\alpha$ S in presence of Hsp27 (5  $\mu\text{M}$ ), under the same condition. (d) disordered U state ( $E_{\text{FRET}} \sim 0.52$ ), and (e) extended helical F state ( $E_{\text{FRET}} \sim 0.15$ ) as predominant conformations of  $\alpha$ S in absence and presence of 500  $\mu\text{M}$  15% PS SUVs, respectively. (f) Shows substantially reduced relative population of the F state of  $\alpha$ S in the presence of Hsp27 (5  $\mu\text{M}$ ), under the same condition.  $\sim 100$  pM of dual labeled  $\alpha\text{S}^{\text{S9C/A85C}}$  (with Alexa488 and Alexa594) were used in these experiments. The solid lines are Gaussian fits of the experimental data. The black line represents the U state only, red line represents the F state only, and the blue line represents the overall population of the  $\alpha$ S species. The peak at zero corresponds to molecules lacking an active acceptor dye. The smFRET histograms are compiled using triplicate data sets.

## **Note S1**

### *Estimation of concentrations of $\alpha$ S and Hsp27 on the SUV surface*

Using experimentally measured diameter of the SUVs (50 nm; Fig. S1), we estimated that each SUV contains approximately 19,500 molecules of lipid monomers using the following formula:

Total number of lipid molecules per vesicle = (Surface area of a SUV/2 x surface per POPG).

(The factor 2 signifies that half of the lipid molecules are on the inner surface of an SUV)

This corresponds to an effective SUV concentration at the highest concentration of lipid used in Fig. 1A (i.e., 1000  $\mu$ M) of  $\sim$  51 nM. Next, we estimated that a maximum of approximately 160  $\alpha$ S and 150 Hsp27 molecules (considering the dimers of Hsp27 as the binding units <sup>[12]</sup>), can independently bind to individual SUVs under saturating conditions, assuming a shell of 5 and 7.7 nm thickness for  $\alpha$ S and Hsp27<sup>[13]</sup>, respectively, on the outer SUV-surface.

Therefore, at the highest concentration of Hsp27 (i.e., 10  $\mu$ M) tested in our ensemble and single-molecule experiments, Hsp27 molecules can effectively occupy > 50% of the available SUV interaction surface at the highest lipid concentration used in our assay (1000  $\mu$ M). Therefore, Hsp27 is effective in inhibiting  $\alpha$ S binding to SUVs by sterically blocking the binding sites due to mass action.

## **Note S2**

### *Characterization of Hsp27-membrane interaction using single-molecule and ensemble fluorescence*

To probe the interaction of Hsp27 with phospholipid vesicles in depth and determine if binding to PG SUVs leads to conformational changes in Hsp27, we employed smFRET experiments. Since Hsp27 has intrinsically disordered N- and C-terminal regions (which accounts for ~ 50% of the protein) and populates large polydisperse oligomers<sup>[12]</sup>, the application of the state-of-the-art smFRET is ideally suited for the conformational analysis of Hsp27 in the free and vesicle-bound states. Using dual-labeled Hsp27<sup>84/173</sup> with the FRET-pair Alexa488/Alexa594, we observed that binding to SUVs are accompanied by a substantial alteration in the conformation of the central conserved  $\alpha$ -crystallin domain of Hsp27 as indicated by the changes in the  $E_{\text{FRET}}$  (Fig. S4a) from 0.82 ( $\pm 0.04$ ) to 0.30 ( $\pm 0.03$ ). The apparent binding affinity estimated from the smFRET histograms (Fig. S4b) agree reasonably well with the ensemble FRET data (Fig. 2B in the *main text*). In addition, we independently measured the binding affinity of the Hsp27 for PG SUVs interaction using the steady state anisotropy of an intrinsic fluorescence reporter, tryptophan (Trp) (Fig S4c). Hsp27 contains five Trp residues localized in the N-terminal region of the protein. Comparable dissociation constants obtained from all these experiments shows that dye-labeling of Hsp27, a necessary modification for ensemble and single-molecule FRET experiments, did not have a significant impact on the affinity of Hsp27-SUV association.

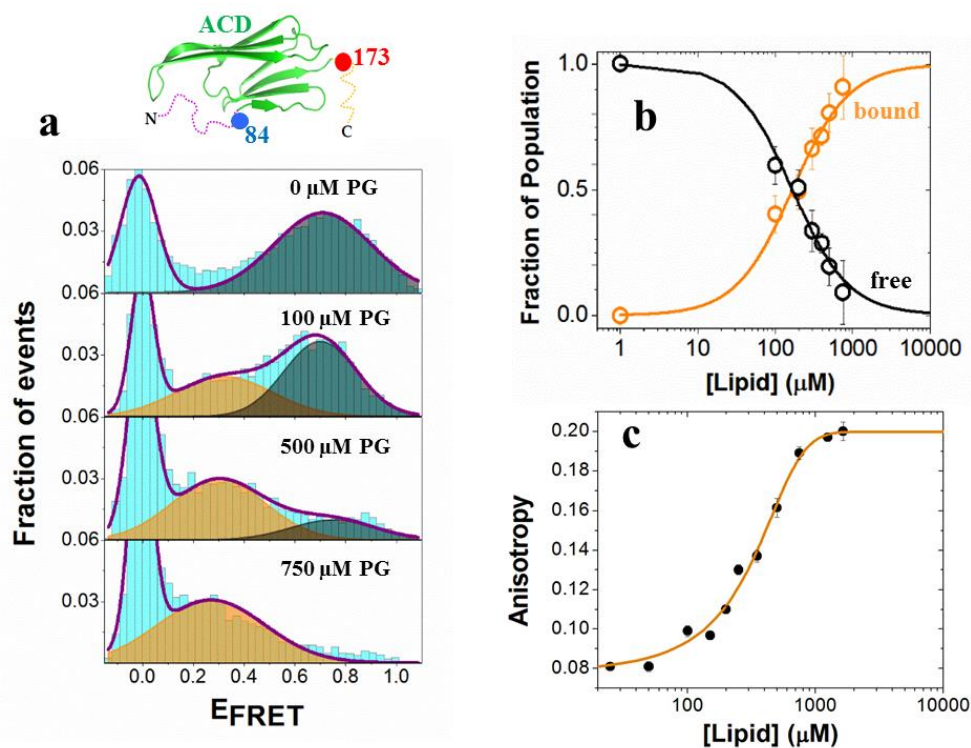


**Figure S4: Characterization of Hsp27-phospholipid vesicle interaction by single-molecule and ensemble fluorescence:** (a) smFRET histograms of dual-labeled Hsp27<sup>84/A173</sup> at increasing [POPG] showing distinct peaks of the free and bound conformational states. Solid lines are Gaussian fits of the data. A cartoon representation of the crystal structure of the truncated ACD domain (PDB ID: 4mjh) with the relative position of the dye-pair being shown at the top (for details, see Note S1). (b) Single-molecule binding isotherm with an observed  $K_D^{\text{Hsp27-lipid}}$  of  $170 \pm 20 \mu\text{M}$ . The smFRET histograms were compiled using triplicate data sets. (c) Apparent binding isotherm of Hsp27-SUV (PG) interaction determined by the changes in the steady state Trp fluorescence anisotropy. The points are the experimental data, the solid line is a fit of the data to a modified Hill equation (equation 4 in the SI Methods), which yielded an apparent dissociation constant ( $K_D^{\text{app}}$ ) of  $239 \pm 69 \mu\text{M}$ .

### **Note S3**

#### *Hsp27 does not interact with the disordered conformation of $\alpha$ -synuclein*

To characterize the mechanistic basis of the inhibitory action of Hsp27 in detail, we also examined whether Hsp27 interacts with the monomeric disordered state of  $\alpha$ S, thereby reducing its affinity for the phospholipid bilayer(s). Using steady-state fluorescence anisotropy measurements on Alexa488-labeled  $\alpha$ S<sup>G7C</sup>, we observed that there is no significant difference in the anisotropy of  $\alpha$ S in the presence and absence of Hsp27, suggesting a lack of interaction between them under the experimental conditions (Fig. S5a). To independently verify this result, we next performed fluorescence correlation spectroscopy (FCS) measurements. The autocorrelation curve for the Alexa488-labeled unbound  $\alpha$ S<sup>G7C</sup>, which gives a direct estimation of the average diffusion time of the  $\alpha$ S molecules through the experimental observation volume, remained unchanged (and hence the diffusion time) in presence of Hsp27 (Fig. S5b). Therefore, our FCS data further reinforce the results from our anisotropy experiments. While the above data suggest a lack of Hsp27- $\alpha$ S interaction, another possibility could be that binding to Hsp27 results in a substantial compaction of the  $\alpha$ S backbone, which might mask changes in its hydrodynamic properties as probed by anisotropy and FCS measurements. To test for this possibility, we performed smFRET experiments with the dual-labeled  $\alpha$ S<sup>9/85</sup> construct. The disordered state (U;  $E_{\text{FRET}} = 0.52 \pm 0.02$ ) remained unaltered in the presence of Hsp27 (Fig. S5c), ruling out this possibility. Therefore, together, our ensemble and single-molecule fluorescence data showed no direct interaction between the natively disordered conformation of  $\alpha$ S and Hsp27 within our experimental resolution. This finding is consistent with the understanding that although IDPs are in general promiscuous binders, they may not have a preference over globular proteins to interact with IDPs *in vivo* <sup>[14]</sup>.

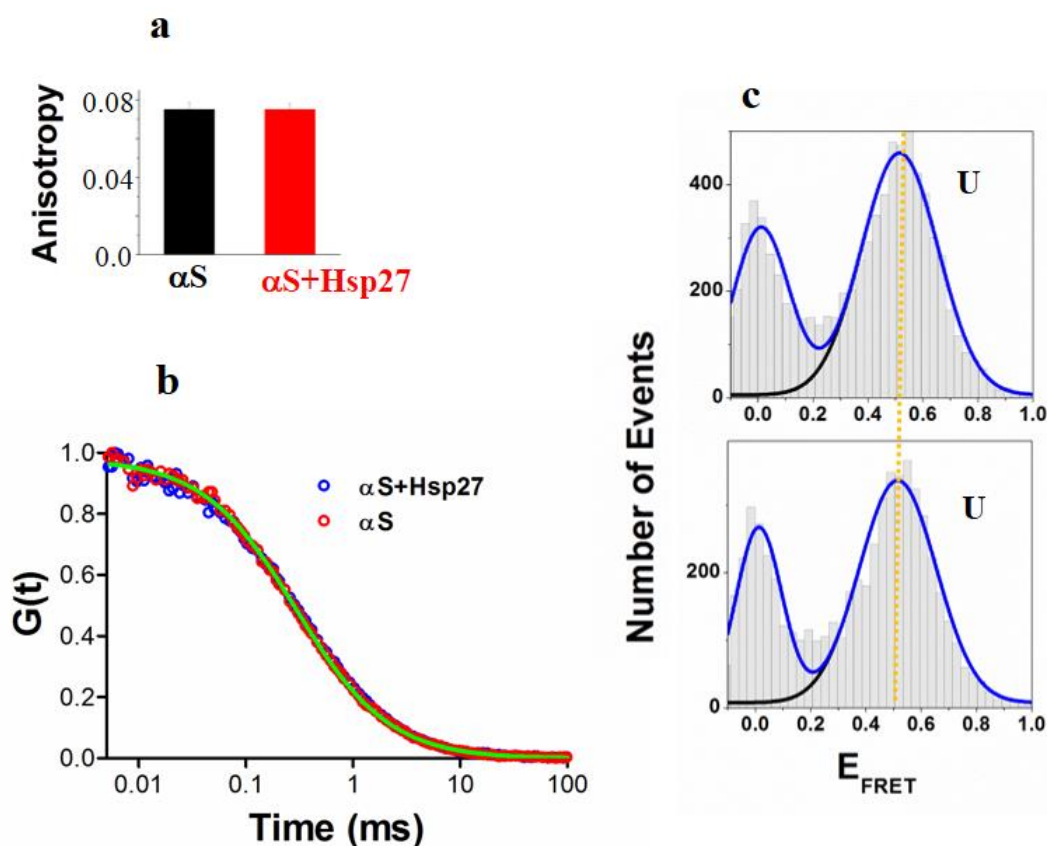
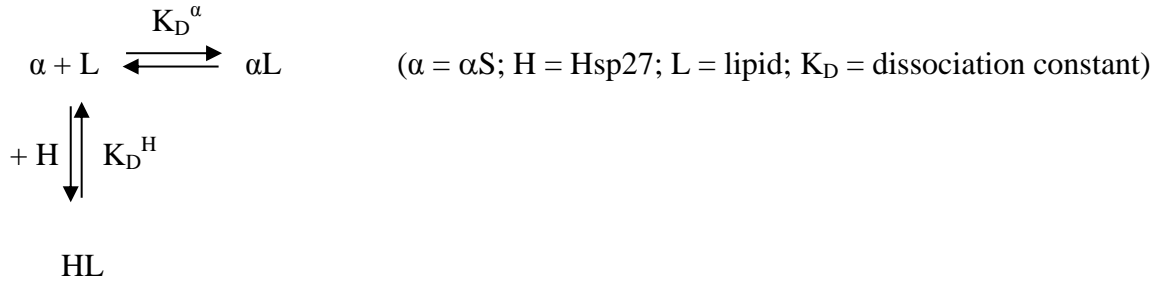


**Figure S5: Hsp27 does not interact with the disordered conformation of  $\alpha S$ : Ensemble experiments.** (a) Steady state fluorescence anisotropy of Alexa594 labeled  $\alpha S^{G7C}$  (1  $\mu\text{M}$ ) in absence and presence of Hsp27 (1:20; mole:mole) showing no significant changes in the anisotropy of  $\alpha S$ . (b) Normalized autocorrelation curves for Alexa488 labeled  $\alpha S^{G7C}$  alone (50 nM, red circles), and in presence of 5  $\mu\text{M}$  Hsp27 (1:20; mole:mole; blue circles) showing no detectable differences. The green line represents a single-component fit of the experimental data using *equation 1* in the Methods. The diffusion times of  $\alpha S$  through the experimental volume were estimated to be  $\sim 250 \mu\text{s}$  in both cases. **Single-molecule experiments.** (c) smFRET histograms showing the disordered, compact native  $\alpha S$  conformation (U state;  $E_{\text{FRET}} \sim 0.52$ ) in absence (top), and presence of 5  $\mu\text{M}$  Hsp27 (bottom) as the predominant conformation of  $\alpha S$ . In these experiments,  $\sim 100 \text{ pM}$  of dual labeled  $\alpha S^{S9C/A85C}$  (with Alexa488 and Alexa594) were used. Solid lines are Gaussian fits of the experimental data. The black line represents U state only. The peak at zero corresponds to molecules lacking an active acceptor dye. Together, these data clearly suggest that Hsp27 does not interact with the disordered conformation of  $\alpha S$ . Error bars represent one sigma ( $\sigma$ ) standard deviation ( $n = 3$ ) in (a). Each autocorrelation curve is an average of 10 data sets in (b). The smFRET histograms are compiled using triplicate data sets in (c).

## Note S4

### Competitive inhibition model for the inhibitory action of Hsp27

Here, we considered a ternary interaction system with  $\alpha$ S (isolated motifs and full-length protein), SUVs and Hsp27 as a third protein component which would compete with  $\alpha$ S for SUV binding, defined as a competitive inhibitor.



### For two component $\alpha$ S-lipid interaction:

$$f_b^\alpha = \frac{[L_{free}]}{K_D^\alpha + [L_{free}]} = \frac{[L_{total}]}{K_D^\alpha + [L_{total}]}; f_b^\alpha = \text{Fraction of } \alpha S \text{ bound} \quad (5)$$

Since,  $[L_{total}] = [L_{free}] + [\alpha L]$ ; and for our experimental conditions,  $[\alpha L] \ll [L_{total}]$

Therefore,  $[L_{total}] \sim [L_{free}]$

### For Hsp27-lipid interaction:

$$K_D^H = \frac{[L_{free}][H_{free}]}{[HL]} = \frac{([L_{total}] - [HL]) \cdot ([H_{total}] - [HL])}{[HL]} \quad (6)$$

Rearranging,

$$[HL]^2 - [HL] ([H_{total}] + [L_{total}] + K_D^H) + [L_{total}][H_{total}] = 0$$

$$\therefore [HL] = \frac{-b - \sqrt{(b^2 - 4ac)}}{2a} \quad (\text{only the negative root is real}^{[15]}) \quad (7)$$

Where,



$$a=1; b=- ([H_{total}] + [L_{total}] + K_D^H); c= [L_{total}][H_{total}]$$

In the presence of Hsp27, eqn. 5 modifies to,

$$f_b^\alpha = \frac{([L_{total}]-[HL])}{K_D^\alpha + ([L_{total}]-[HL])} \quad (8)$$

Equation (8) describes the variation of the fraction of  $\alpha$ S (bound) with  $[L_{total}]$  at any given  $[H_{total}]$  and shows a hyperbolic curve saturating at  $f_b^\alpha = 1.0$  (Fig. S6a). It also reveals that the binding isotherm “slides” to the right as a function of  $[Hsp27]$  (or  $[H_{total}]$ ). The value of  $[L_{total}]$  at which  $f_b^\alpha = 0.50$ , i.e., the apparent  $K_D^\alpha$ , increases monotonically (as indicated with a *horizontal line* in Fig. S6a). When we plotted the apparent  $K_D^\alpha$  vs  $[H_{total}]$ , a linear relationship was observed (Fig. S6b). This linearity is a benchmark of *unimodal inhibition* in which the inhibitor competitively inhibits protein-ligand interaction involving only one mode. Moreover, the slope of the straight line ( $m$  value) is characteristic of the inhibition efficacy by the inhibitor, and dependent on the ratio of  $K_D^\alpha$  and  $K_D^H$ .

In case of a bimodal protein-lipid interaction with one weak and one strong mode of interactions, (i.e., two  $K_D^\alpha$  values are significantly different), the slopes of the individual  $K_D^\alpha$  vs  $[H_{total}]$  lines vary greatly (S7b), signifying distinct efficiencies of inhibition for individual mode of interactions. In this case, our simulation reveals that the ratio of the two dissociation constants ( $K_D^{\alpha 1}$  and  $K_D^{\alpha 2}$ ) steeply rises with increasing  $[H_{total}]$ , and saturates at a value equal to  $m_{a1}/m_{a2}$  (i.e., the ratio of the slopes of the inhibition lines; Fig. S6c). This results in a significant increase in the population of the state where the stronger binding has exclusively favored (herein termed as “hidden state”) as a function of  $[H_{total}]$ . In the present case, as a result of the *bimodal inhibition*, the inhibitor (Hsp27) amplifies the population of the hidden state from ~15% to ~70% under the present conditions (Fig. S6c).

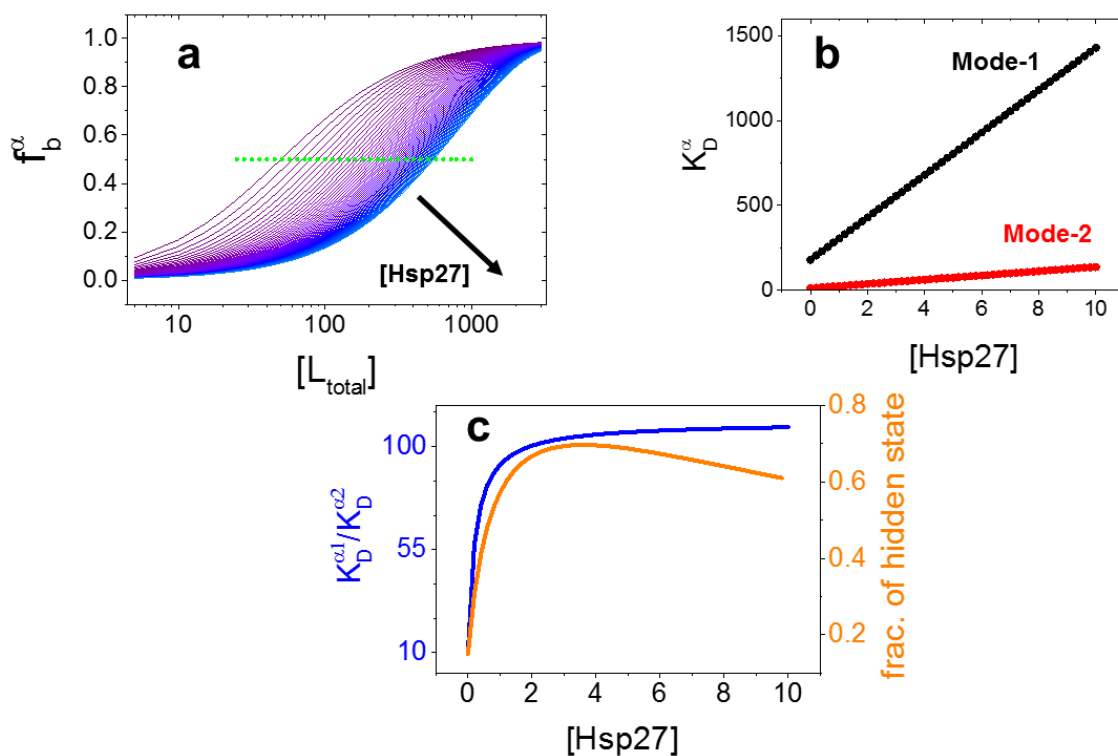


**Figure S6: Competitive inhibition model.** (a) Numerical simulation of the competitive inhibition model based on eqns. (7) and (8). The binding isotherms “slide” to the right with increasing  $[Hsp27]$ . The horizontal green dotted line corresponds to  $f_b^\alpha = 0.50$ , showing a steady shift in the apparent  $K_D^\alpha$ . (b) Plot showing a linear relationship between the  $K_D^\alpha$  vs.  $[H_{total}]$ , which is a benchmark of *unimodal* inhibition (axes are in  $\mu\text{M}$  units). Shown here are two modes of  $\alpha\text{S}$  binding to membranes, with *mode-1* being  $\sim 15$  fold weaker than the *mode-2*. This graph also reveals a dramatic difference in the individual slopes ( $\sim 100$  fold). (c) Variation of the ratio of individual  $K_D^\alpha$  for *mode-1* and *mode-2* with the  $[Hsp27]$ . The curve saturates at  $m_{\alpha1}/m_{\alpha2}$  (i.e., the ratio of the slopes of the inhibition lines from b). Also shown the variation of the “hidden state” population in the same graph (*right axis, orange*), revealing a sharp increase followed by a weak decrease after passing through a maximum. The following values are used for this simulation (as measured by experiments reported here):  $K_D^{\alpha1}$  and  $K_D^{\alpha2}$  in absence of Hsp27 = 180 and 12.5  $\mu\text{M}$ , respectively;  $K_D^H = 200 \mu\text{M}$ ; number of lipids per Hsp27 ( $n$ ) = 250 (as estimated in Note S1).

A comparison of our experimental data (reported in *Figure-1B* in the main text) with the simulated results using competitive inhibition model shows a clear deviation of the experimentally measured dissociation constants ( $K_D^\alpha$ ) vs.  $[H_{total}]$  from linearity. Therefore, a unimodal competitive inhibition

model is not adequate to completely describe the mechanism of the observed inhibition by Hsp27 for  $\alpha$ S. We hypothesize that the deviation is a result of *bimodal membrane binding of  $\alpha$ S*, with two different lipid binding modes vastly differing in binding affinities. Hsp27 may have differential inhibition efficacy towards each of individual binding modes (Fig. S6b). In that case, the observed  $K_D^\alpha$  represents a weighted average of the two modes of binding, and the effect of Hsp27 on the individual  $K_D^\alpha$  is dependent upon  $[H_{total}]$  (Fig. S7). In support of this argument, we also have studied  $\alpha$ S fragments corresponding to two membrane interacting helices of  $\alpha$ S, and observed that the inhibition data for individual helices can be well described by a linear  $K_D^\alpha$  vs  $[H_{total}]$  relationship (Fig. 3A,B in *main text*). The numerical simulation is shown below.

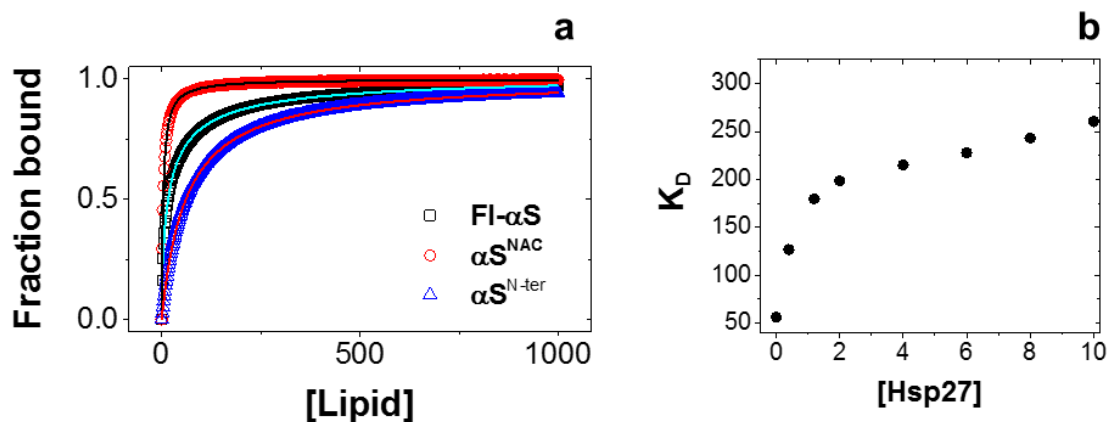


**Figure S7: Numerical simulation of the bimodal membrane binding of  $\alpha$ S.** (a) Binding isotherms (red and blue traces) describing the SUV binding of  $\alpha$ S<sup>NAC</sup> and  $\alpha$ S<sup>N-ter</sup>, respectively. The simulation was done using the experimentally determined  $K_D$  values for the individual fragments (see Fig. 3; *main text*) and using Eqn. 5. The black trace is a simulated bimodal binding curve ( $\sum f_b^{\alpha S} = \frac{[L]}{K_D^\alpha + [L]}$ ) with two  $K_D$  values corresponding to the individual fragments (assuming an equal weightage). An apparent  $K_D$  value of 62  $\mu$ M was obtained after fitting this simulated curve to Eqn. 5, which closely matches with the experimentally determined value of 49.88 ( $\pm$  10.96)  $\mu$ M. (b) Simulation of apparent  $K_D$  as a function of Hsp27 concentration (assuming the Hill coefficient ( $n$ ) = 1). This is done using the  $K_D$  values for the fragments at different  $[Hsp27]$ , calculated from the experimentally determined inhibition efficacy (slopes,  $m_{\alpha S-N-ter}$  and  $m_{\alpha S-NAC}$  of linear plots in Fig. 3), followed by simulation of the individual bimodal binding curves (as shown in (a)). Since  $m_{\alpha S-N-ter}/m_{\alpha S-NAC} \sim 100$ ,  $K_D^{\alpha S-N-ter}/K_D^{\alpha S-NAC}$  asymptotically increases from  $\sim 15$  to the value given by  $m_{\alpha S-N-ter}/m_{\alpha S-NAC}$  as a function of  $[Hsp27]$ .

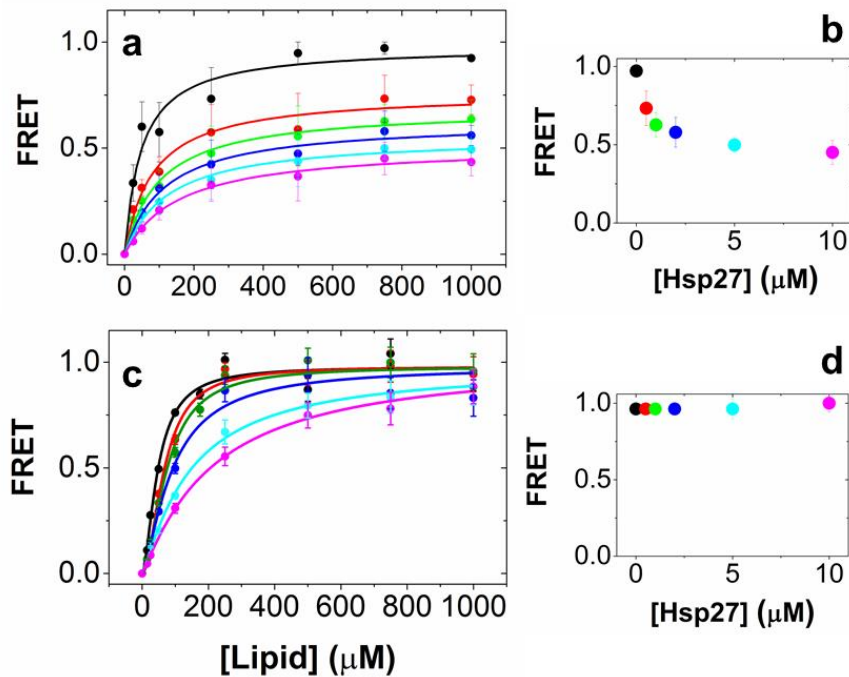


**Figure S8: Hsp27 differentially modulates the membrane interaction of the  $\alpha\text{S}^{\text{N-ter}}$  and  $\alpha\text{S}^{\text{NAC}}$  in the full-length protein.** (a) SUV-to- $\alpha\text{S}$  FRET assay with Alexa594- $\alpha\text{S}^{\text{FL-G7C}}$  as a probe for the N-terminal helix in the full-length protein. Increasing [Hsp27] results in sliding of the binding curves towards higher apparent  $K_D$ 's, and a decrease in the FRET efficiencies at the end baseline. This is shown in (b). (c) SUV-to- $\alpha\text{S}$  FRET with Alexa594- $\alpha\text{S}^{\text{FL-G84C}}$  as a probe for the central helix. Increasing [Hsp27] results in a shift of the binding curves towards higher apparent  $K_D$ 's, without any significant change in the FRET efficiencies at the end baseline. This is shown in (d). Color code: *black*-0  $\mu\text{M}$  Hsp27; *red*- 0.5  $\mu\text{M}$  Hsp27; *green*-1  $\mu\text{M}$  Hsp27; *blue*-2  $\mu\text{M}$  Hsp27; *cyan*-5  $\mu\text{M}$  Hsp27; *magenta*-10  $\mu\text{M}$  Hsp27.

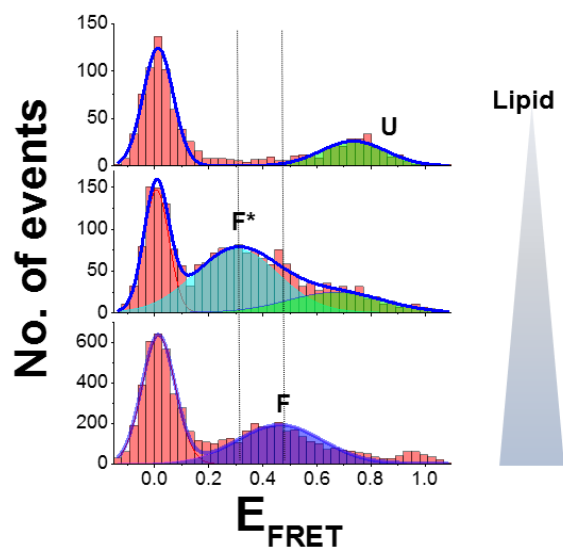


**Figure S9: A hidden conformation of  $\alpha\text{S}$  on the lipid bilayer.** (a) smFRET histograms of the dual-labeled  $\alpha\text{S}^{3/51\text{C}}$  showing a hidden conformational state (F\*) at a very low lipid concentration (5  $\mu\text{M}$  PG; middle panel). The extended helical F state is predominantly observed at higher than 50  $\mu\text{M}$  PG. Also shown here are representative histograms of the U state (0  $\mu\text{M}$  PG; upper panel) and F state at 250  $\mu\text{M}$  PG (lower panel).

**Table S1**

[Hsp27] ( $\mu\text{M}$ )	$K_D^{\text{app}}$ (ensemble anisotropy) ( $\mu\text{M}$ )	$K_D^{\text{app}}$ (smFRET) ( $\mu\text{M}$ )	$K_D^{\text{app}}$ (vesicle-to-protein FRET; $\alpha\text{S}^{\text{F1-G7C}}$ ) ( $\mu\text{M}$ )	$K_D^{\text{app}}$ (vesicle-to-protein FRET; $\alpha\text{S}^{\text{F1-G84C}}$ ) ( $\mu\text{M}$ )
0	49.88 ( $\pm 10.96$ )	39.90 ( $\pm 18.59$ )	47.93 ( $\pm 11.50$ )	47.46 ( $\pm 5.44$ )
1	87.08 ( $\pm 10.07$ )	109.79 ( $\pm 10.50$ )	99.95 ( $\pm 10.60$ )	74.30 ( $\pm 4.38$ )
1.5	121.04 ( $\pm 19.51$ )	n.d.*	n.d.	n.d.
2	n.d.	n.d.	114.25 ( $\pm 15.23$ )	90.57 ( $\pm 11.38$ )
2.5	192.49 ( $\pm 27.57$ )	n.d.	n.d.	n.d.
4	230.01 ( $\pm 24.11$ )	n.d.	n.d.	n.d.
5	248.19 ( $\pm 28.73$ )	256.66 ( $\pm 66.61$ )	123.19 ( $\pm 13.17$ )	145.76 ( $\pm 5.29$ )
7.5	288.12 ( $\pm 21.73$ )	n.d.	n.d.	n.d.
10	306.02 ( $\pm 29.40$ )	n.d.	156.25 ( $\pm 20.33$ )	212.97 ( $\pm 30.41$ )

Estimated dissociation constants of  $\alpha\text{S}$ -SUV (POPG) interaction using ensemble and single-molecule experiments (\* n.d. = not determined). Errors ( $\sigma$ ) are indicated in the parenthesis.

## Supplementary References

- [1] A. Rekas, C. G. Adda, J. Andrew Aquilina, K. J. Barnham, M. Sunde, D. Galatis, N. A. Williamson, C. L. Masters, R. F. Anders, C. V. Robinson, R. Cappai, J. A. Carver, *J Mol Biol* **2004**, *340*, 1167-1183.
- [2] A. C. Ferreon, A. A. Deniz, *Biochemistry* **2007**, *46*, 4499-4509.
- [3] A. C. Ferreon, Y. Gambin, E. A. Lemke, A. A. Deniz, *Proc Natl Acad Sci U S A* **2009**, *106*, 5645-5650.
- [4] P. R. Banerjee, D. M. Mitrea, R. W. Kriwacki, A. A. Deniz, *Angew Chem Int Ed Engl* **2016**, *55*, 1675-1679.
- [5] M. P. Bova, H. S. McHaourab, Y. Han, B. K. Fung, *J Biol Chem* **2000**, *275*, 1035-1042.
- [6] A. C. Ferreon, J. C. Ferreon, P. E. Wright, A. A. Deniz, *Nature* **2013**, *498*, 390-394.
- [7] S. Mukhopadhyay, R. Krishnan, E. A. Lemke, S. Lindquist, A. A. Deniz, *Proc Natl Acad Sci U S A* **2007**, *104*, 2649-2654.
- [8] D. Pristiniski, V. Kozlovskaya, S. A. Sukhishvili, *The Journal of chemical physics* **2005**, *122*, 14907.
- [9] J. N. Weiss, *FASEB J* **1997**, *11*, 835-841.
- [10] M. Haslbeck, T. Franzmann, D. Weinfurtner, J. Buchner, *Nat Struct Mol Biol* **2005**, *12*, 842-846.
- [11] R. Shashidharamurthy, H. A. Koteiche, J. Dong, H. S. McHaourab, *J Biol Chem* **2005**, *280*, 5281-5289.
- [12] H. S. McHaourab, J. A. Godar, P. L. Stewart, *Biochemistry* **2009**, *48*, 3828-3837.
- [13] a) S. Jehle, B. S. Vollmar, B. Bardiaux, K. K. Dove, P. Rajagopal, T. Gonen, H. Oschkinat, R. E. Kleivit, *Proc Natl Acad Sci U S A* **2011**, *108*, 6409-6414; b) C. Galvagnion, A. K. Buell, G. Meisl, T. C. Michaels, M. Vendruscolo, T. P. Knowles, C. M. Dobson, *Nat Chem Biol* **2015**, *11*, 229-234.
- [14] H. Hegyi, P. Tompa, *PLoS Comput Biol* **2008**, *4*, e1000017.
- [15] M. A. Williams, *Methods Mol Biol* **2013**, *1008*, 3-34.